

1 **Supplementary Information**

2

3 **ClusterMap for multi-scale clustering analysis of spatial gene expression**

4

5 **Yichun He^{1,2,8}, Xin Tang^{1,2,8}, Jiahao Huang², Jingyi Ren^{2,3}, Haowen Zhou², Kevin Chen⁴,**

6 **Albert Liu^{2,3}, Hailing Shi^{2,3}, Zuwan Lin^{4,2}, Qiang Li¹, Abhishek Aditham^{2,5}, Johain**

7 **Ounadjela^{2,6}, Emanuelle I Grody^{2,6}, Jian Shu^{2,6,7}, Jia Liu^{1*} & Xiao Wang^{2,3*}**

8

9 ¹John A. Paulson School of Engineering and Applied Sciences, Harvard University, Cambridge,
10 MA, USA.

11 ²Broad Institute of MIT and Harvard, Cambridge, MA, USA.

12 ³Department of Chemistry, Massachusetts Institute of Technology, Cambridge, MA, USA.

13 ⁴Department of Chemistry and Chemical Biology, Harvard University, Cambridge, MA, USA.

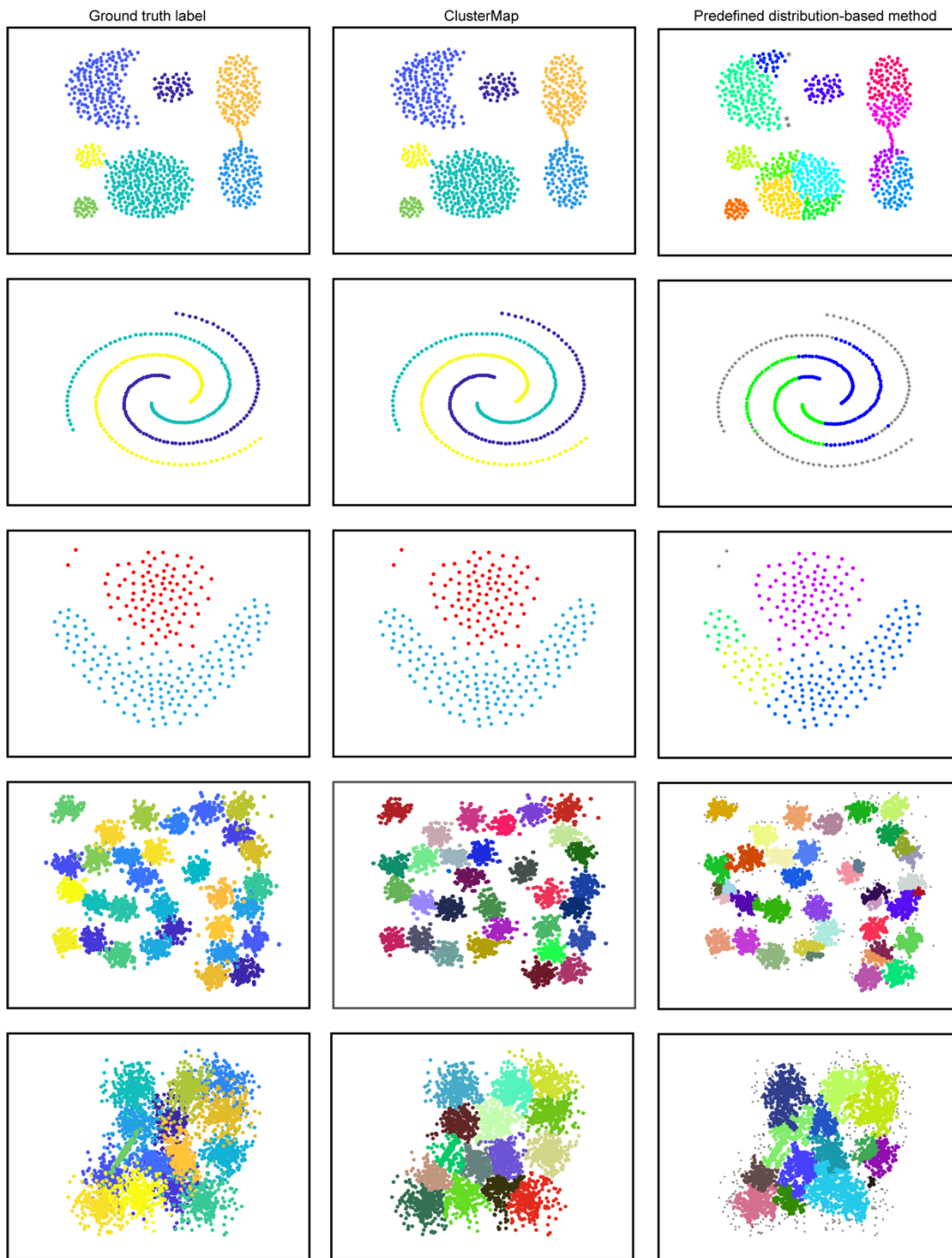
14 ⁵Department of Biological Engineering, Massachusetts Institute of Technology, Cambridge, MA,
15 USA.

16 ⁶Whitehead Institute for Biomedical Research, Cambridge, MA, USA.

17 ⁷Cutaneous Biology Research Center, Massachusetts General Hospital, Harvard Medical School,
18 Boston, MA, USA.

19 ⁸These authors contributed equally: Yichun He, Xin Tang.

20 *e-mail: wangxiao@broadinstitute.org; jia_liu@seas.harvard.edu.



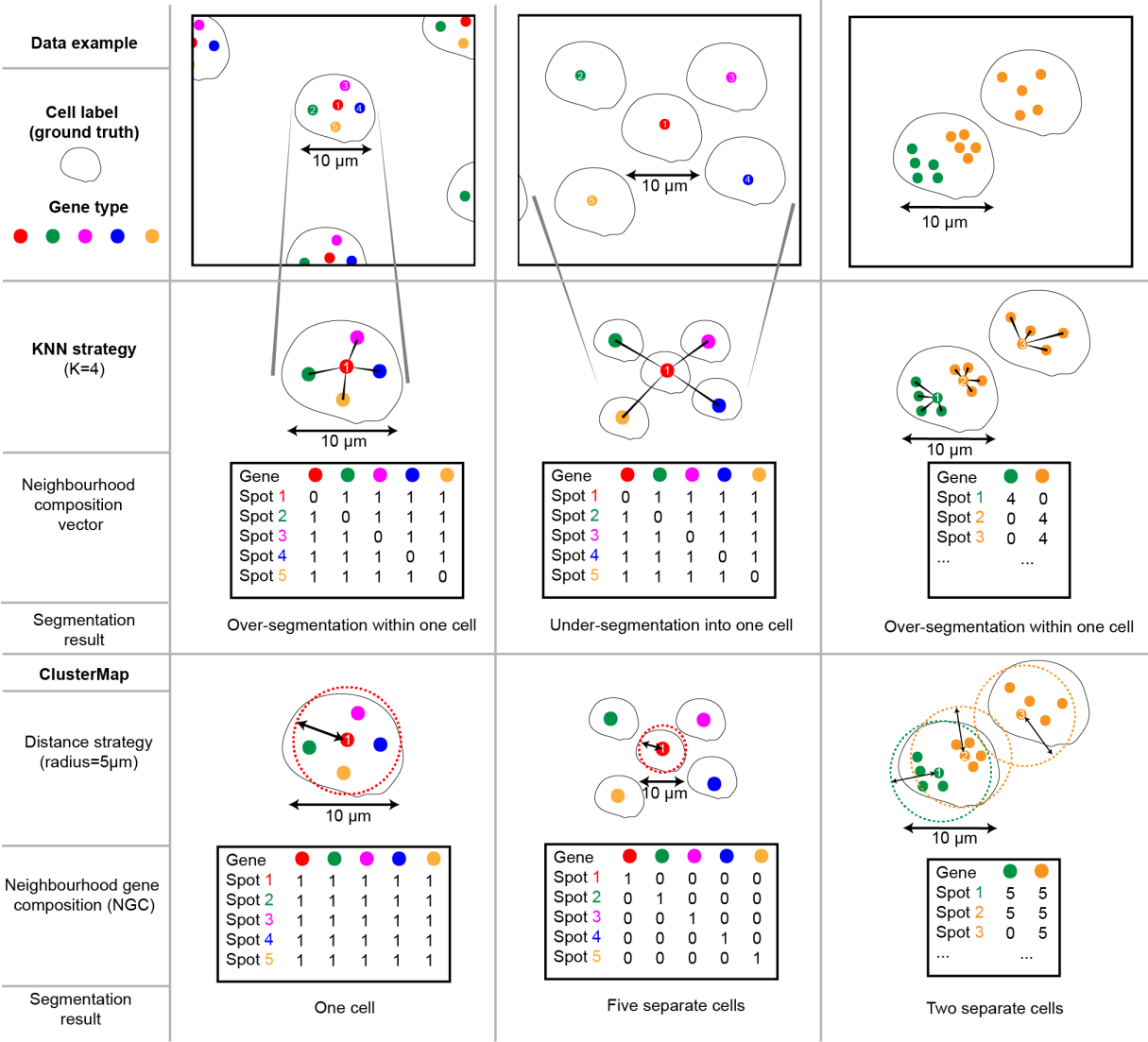
22 **Supplementary Figure 1**

23 **Performance comparison of ClusterMap and predefined distribution-based method in**

24 **simulated data.** Different colors represent different segmentation results. Note that the gene

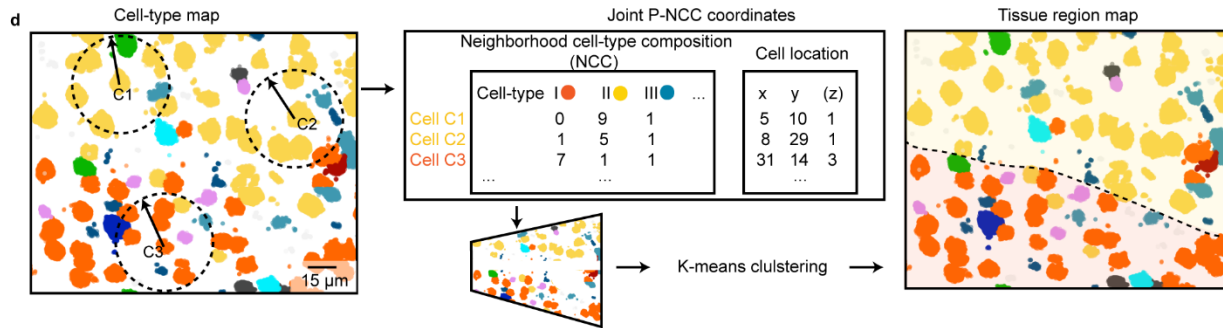
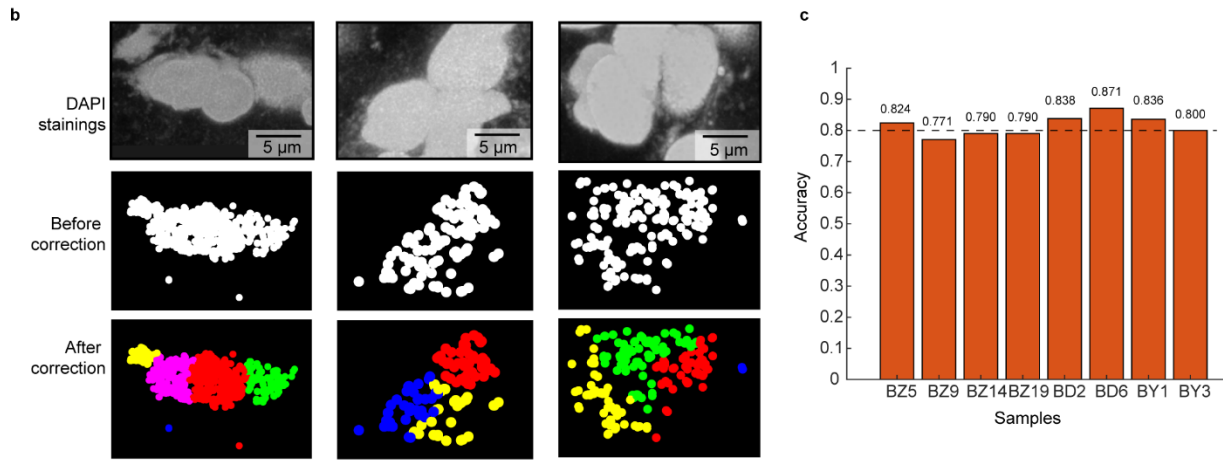
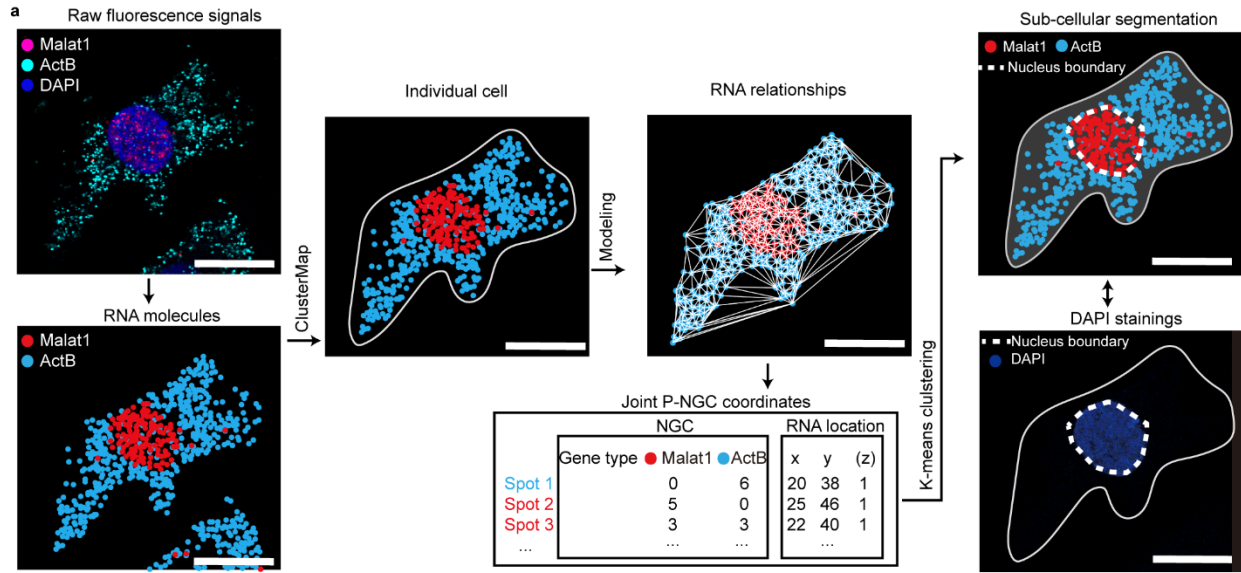
25 identity of each spot is randomly assigned from 1 to 5 as pseudo gene type. Left: ground truth;

26 Middle: ClusterMap results; Right: results using predefined distribution-based method²⁰.



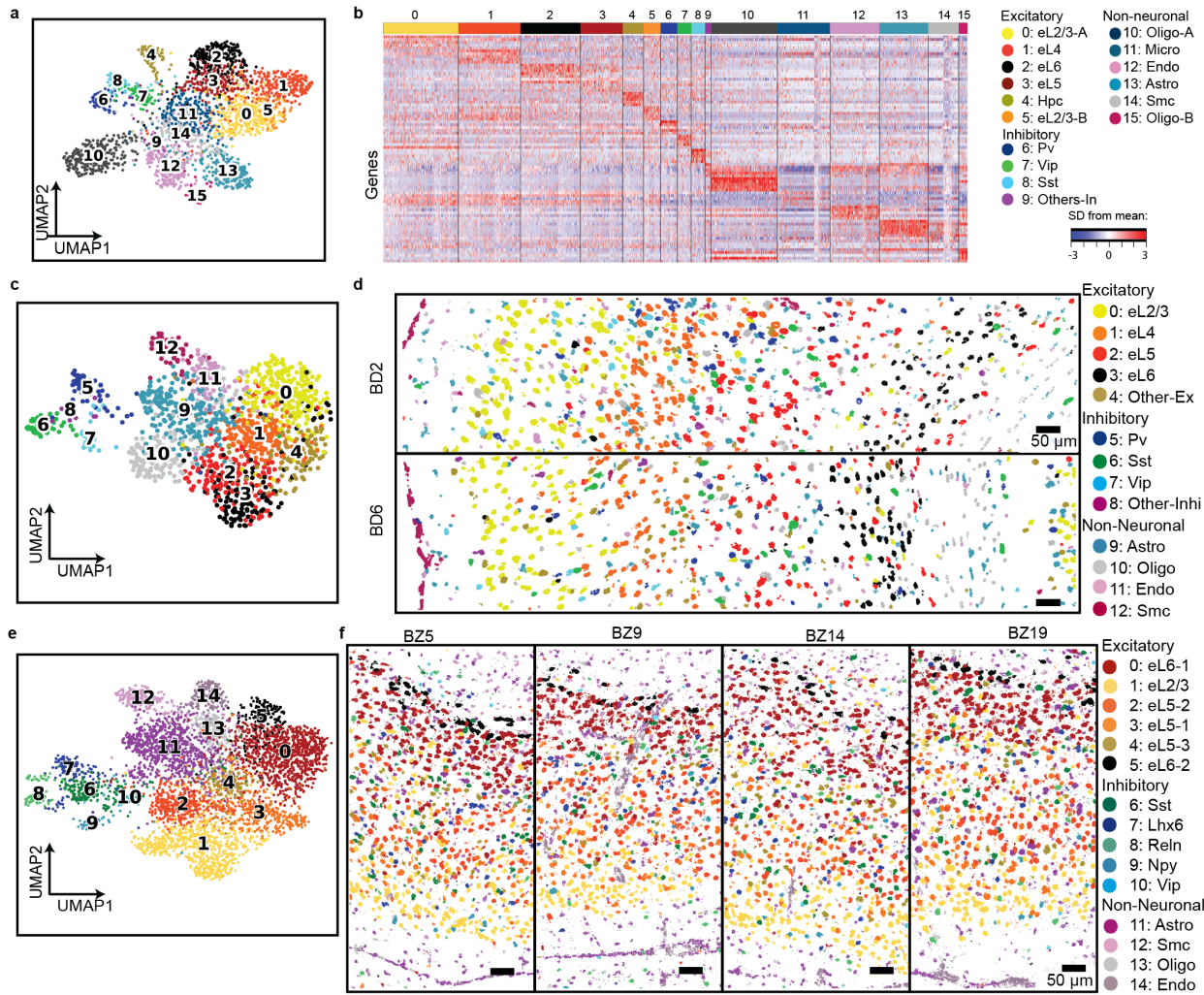
29 **Supplementary Figure 2**

30 **Comparison of RNA sampling approaches between ClusterMap using absolute physical**
31 **distance with other methods²⁰ using k -nearest neighbours (kNN) in simulated data.** Three
32 examples of RNAs with various local density demonstrating that ClusterMap preserves the local
33 physical density information while kNN does not consider the physical density of RNAs.



36 **Supplementary Figure 3**

37 **Illustration of sub-cellular, cellular, and tissue region analyses.** **a**, Subcellular analysis process
38 of the panel IV in **Figure 1d** by ClusterMap. A three-channel (magenta: *Malat1*; cyan: *ActB*; blue:
39 DAPI) composite image shows raw fluorescent signals. After preprocessing mRNA molecules
40 with specific genes located, ClusterMap first performs cellular resolution and identifies individual
41 cells. Then a mesh graph that models the relationships among mRNA spots in the cell is generated
42 to compute the NGC coordinates and *K*-means clustering separate spots into two regions using
43 joint physical and NGC coordinates. 100 times *K*-means clustering was performed with different
44 seeds and showed the consistent same results. Finally, a convex hull is constructed from the
45 nucleus spots, denoting the nucleus boundary. The pattern of ClusterMap-constructed nucleus
46 boundary is compared with the DAPI staining. Scale bar: 20 μ m. **b**, Examples of the cell
47 identification in ClusterMap procedures in **Fig. 2a**. Upper: DAPI staining showing the cell nuclei.
48 Middle: mRNA spots. Lower: Clustering results. **c**, The accuracy of cell identification results from
49 eight STARmap⁶ datasets compared with corresponding expert-annotated labels. BZ5, BZ9, BZ14,
50 BZ19: four STARmap⁶ 166-gene sets in mouse medial prefrontal cortex (mPFC); BD2, BD6: two
51 STARmap⁶ 160-gene sets in mouse V1. BY1, BY3: two STARmap 1020-gene sets in mouse V1.
52 The horizontal line is at 80% accuracy. **d**, ClusterMap constructs the tissue regions after cell-typing.
53 First, the neighborhood cell-type composition (NCC) of each cell is computed by considering a
54 sliding window over the cell-type map. Then both the NCC and physical locations of cells are
55 combined for *K*-means clustering. Cells with highly correlated neighboring cell-type composition
56 and close spatial distances are merged into a single tissue region signature.



59 **Supplementary Figure 4**

60 **Identification of cell types in mouse primary cortex (V1) and medial prefrontal cortex**

61 **(mPFC). a,b**, UMAP and heatmap visualization of all excitatory, inhibitory and non-neuronal cell

62 types in STARmap⁶ mouse V1 1020-gene (two replicates: BY1 and BY3). The heatmap represents

63 z-scored expression matrix of all cell types, showing clustering of five most differentially

64 expressed genes per cell type. Genes shown are selected based on a false discovery rate (FDR)-

65 adjusted *p*-value threshold of 0.05 (Benjamini-Hochberg correction) and a minimum *log*₁₀ fold

66 change of 0.4, using a two-sided, unpaired t-test, for genes that are expressed in cells within each

67 cluster versus cells in any other cluster. **c, e**, UMAP visualization of all excitatory, inhibitory and

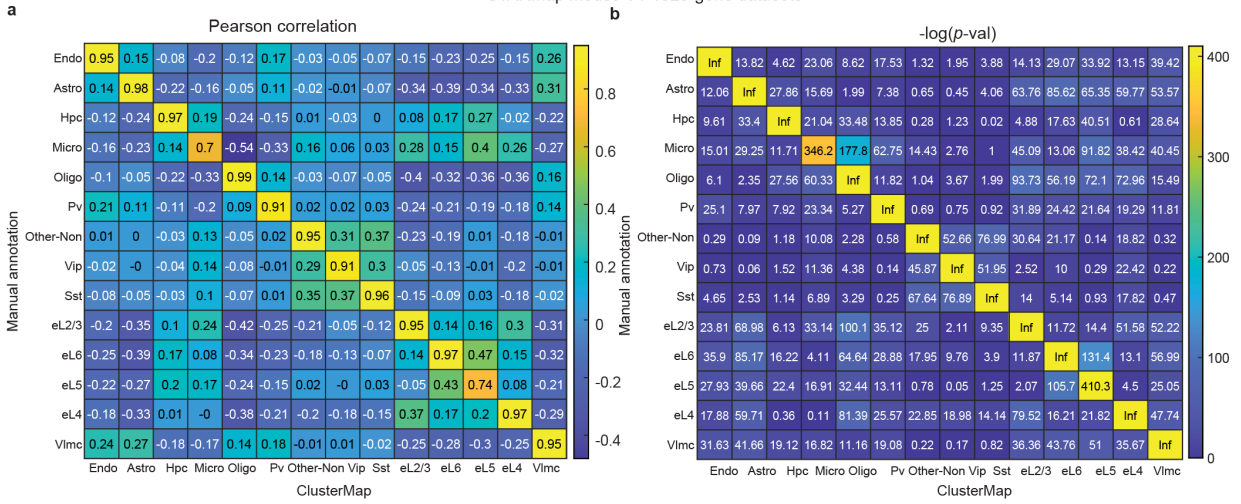
68 non-neuronal cell types in STARmap⁶ 160-gene datasets in mouse V1 (two replicates: BD2, BD6,

69 **(c)**), and STARmap⁶ 166-gene datasets in mPFC (four replicates, BZ5, BZ9, BZ14, BZ19, **(e)**).

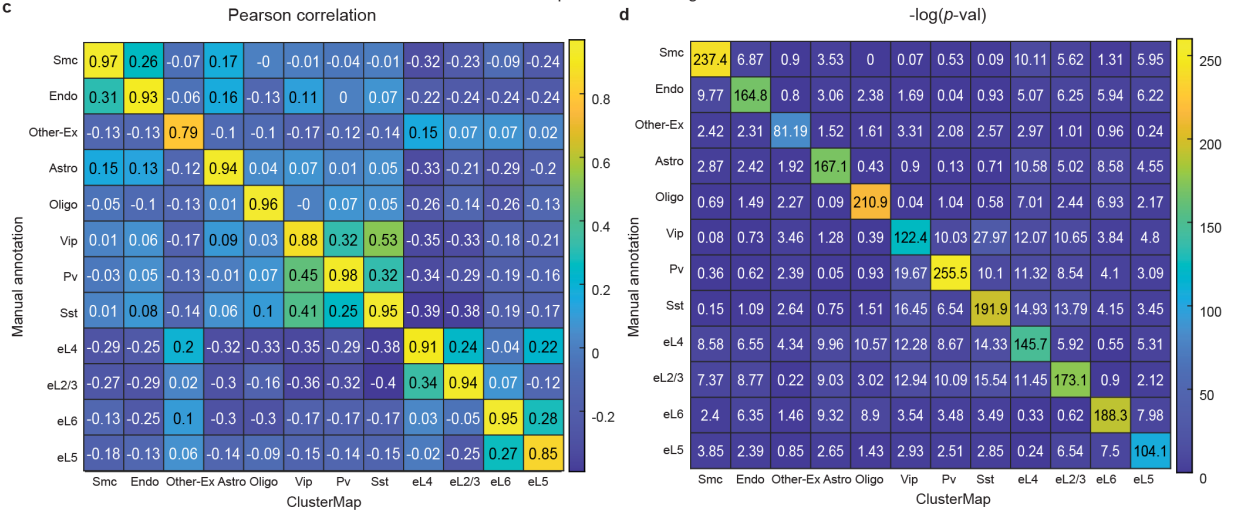
70 **d, f**, Spatial organization map of cell types in BD2 and BD6 **(d)**, and in BZ5, BZ9, BZ14 and BZ19

71 **(f)**.

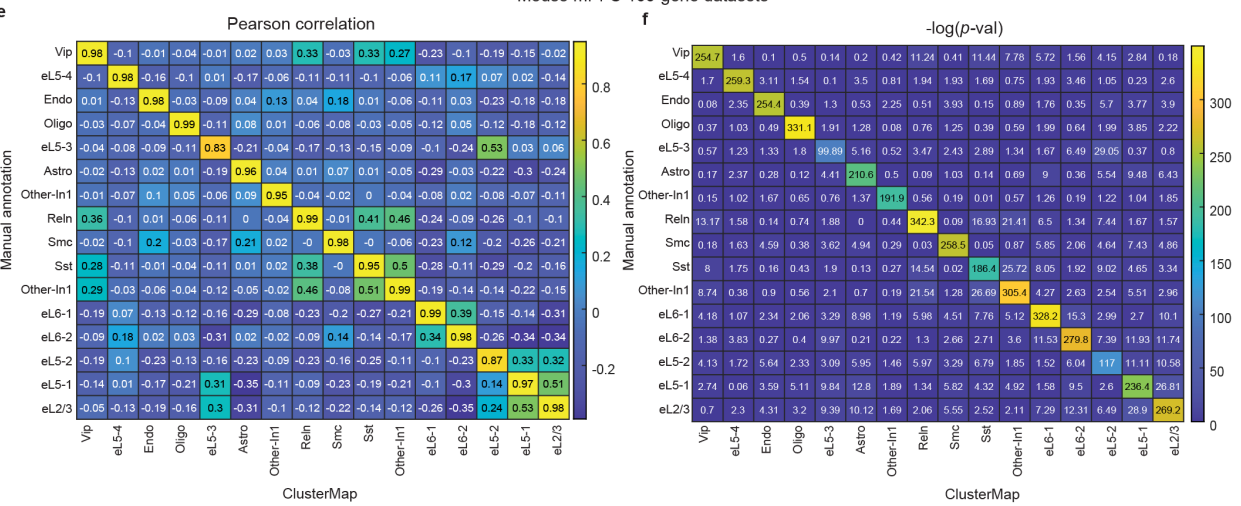
STARmap mouse V1 1020-gene datasets



STARmap mouse V1 160-gene datasets



Mouse mPFC 166-gene datasets



73 **Supplementary Figure 5**

74 **Cell-type correlation matrices comparison of ClusterMap-based and manually-segmented**

75 **cell types. a,b**, Comparison on STARmap mouse V1 1020-gene datasets. Heatmaps of Pearson

76 correlation (**a**) and $-\log(p\text{-value})$ (**b**) for null hypothesis testing. The p value is based on a t statistic

77 which has $n-2$ degrees of freedom and 95% confidence interval. The single-cell gene expression

78 profiles from ClusterMap with manual annotation are compared. **c,d**, Comparison on STARmap

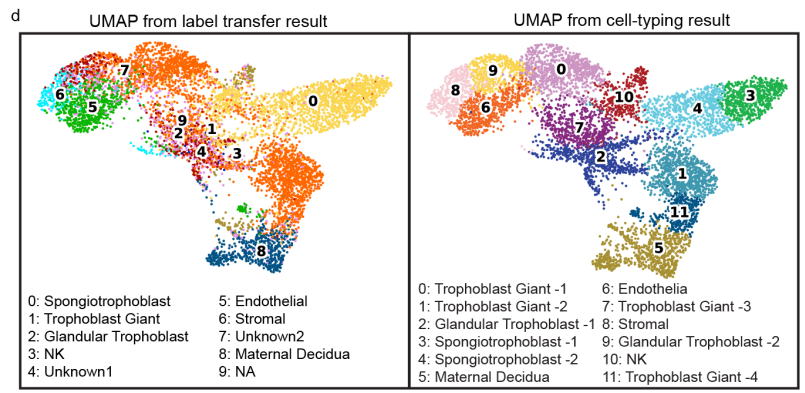
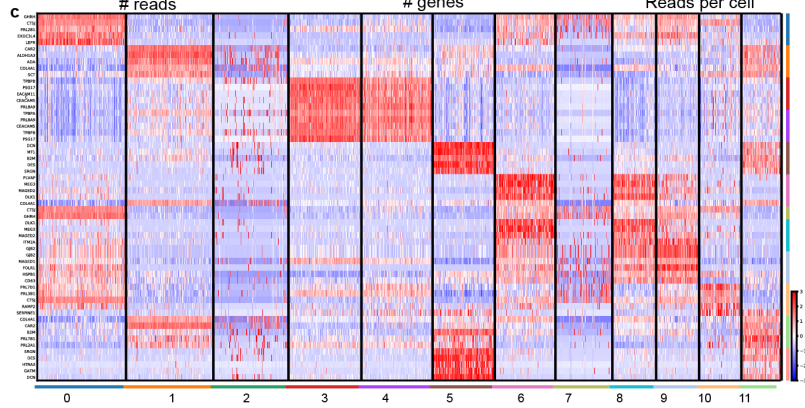
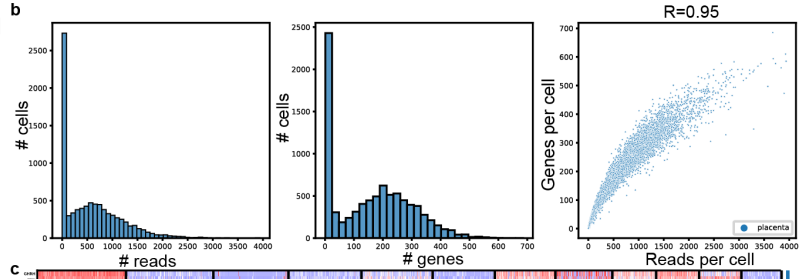
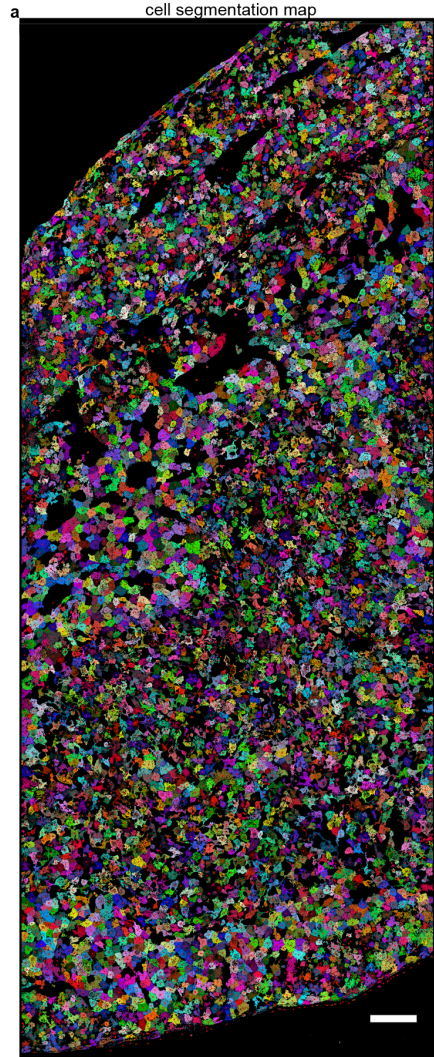
79 mouse V1 160-gene datasets. Heatmaps of correlation (**c**) and $-\log(p\text{-value})$ (**d**) comparing the

80 single-cell gene expression profiles from ClusterMap with manual annotation. **e,f**, Comparison on

81 STARmap mouse mPFC 166-gene datasets. Heatmaps of correlation (**e**) and $-\log(p\text{-value})$ (**f**)

82 comparing the single-cell gene expression profiles from ClusterMap with manual annotation.

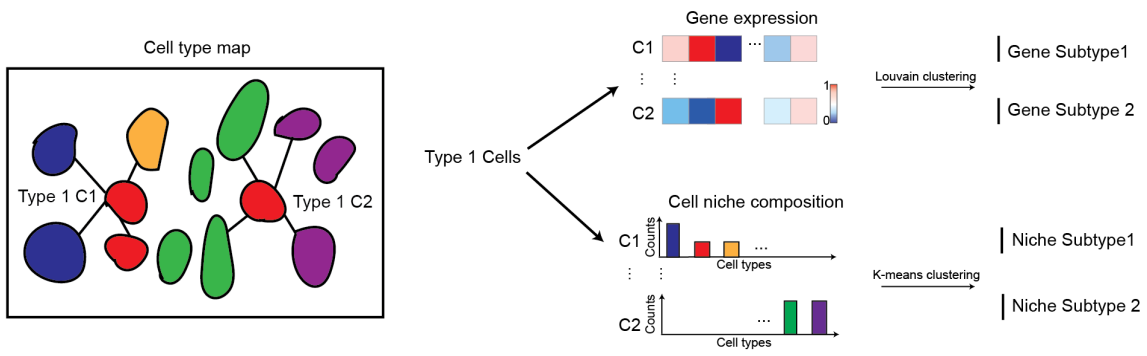
83 Horizontal: ClusterMap; vertical: manual annotation.



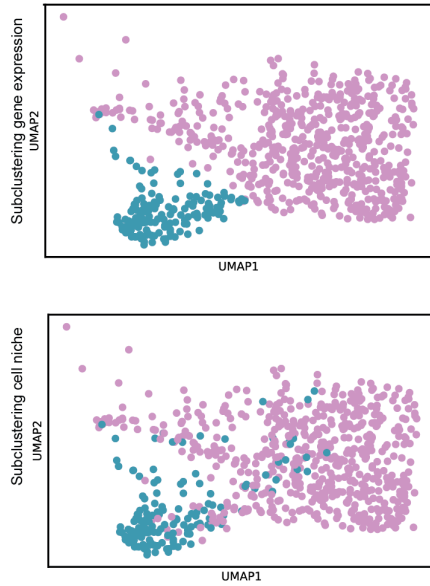
85 **Supplementary Figure 6**

86 **Analyses of the STARmap⁶ mouse placental dataset.** **a**, ClusterMap generates the cell
87 segmentation map of the STARmap⁶ mouse placenta 903-gene dataset, including 7,224 cells. Scale
88 bar: 100 μm . **b**, Statistics of ClusterMap identified placental cells as shown in **(a)**. Left: Histogram
89 of detected reads (DNA amplicons) per cell. Middle: Histogram of genes per cell. Right:
90 Correlation plot between genes per cell and reads per cell. **c**, Heatmap visualization of 12 cell types.
91 Names are in the right panel of **(d)**. **d**, UMAP from label transfer results with scRNA-seq,
92 compared with UMAP of the Louvain clustering²² in ClusterMap.

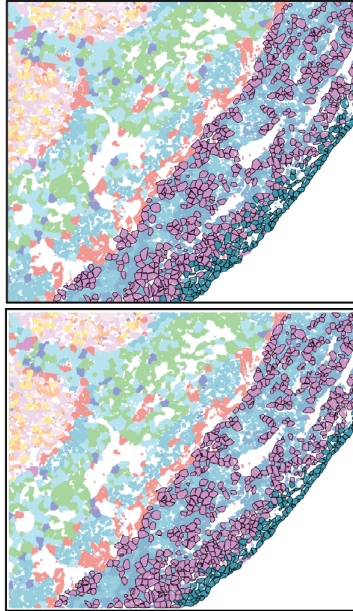
a



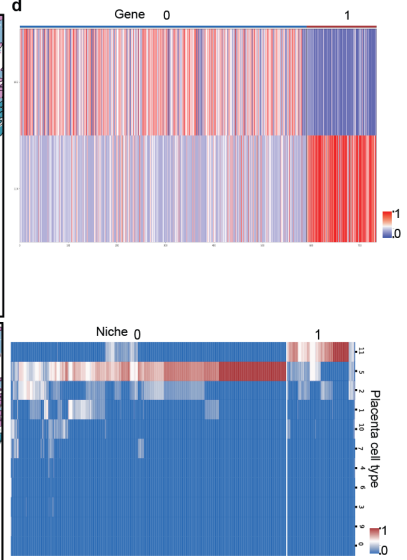
b



c



d



94 **Supplementary Figure 7**

95 **Sub-clustering within one cell type using cell niche compositions in STARmap mouse**

96 **placenta 903-gene dataset. a**, Schematic indicating how cells in one cell type are sub-clustered

97 based on either gene expression (Louvain clustering²²) or the cell niche compositions (*K*-means

98 clustering¹⁹). **b**, UMAP of gene expression sub-clustering (top) or cell niche composition sub-

99 clustering (bottom) in Maternal Decidua-1 (MD-1). **c**, Spatial subtype maps using gene expression

100 (top) or cell niche composition (bottom) in MD-1. **d**, Heatmap of sub-clustering using gene

101 expression (top) or cell niche composition sub-clustering (bottom) in MD-1. Gene markers in the

102 top heatmaps of gene expression sub-clustering are 0: *GPNMB*, 1: *CXCL14*. Row names in the

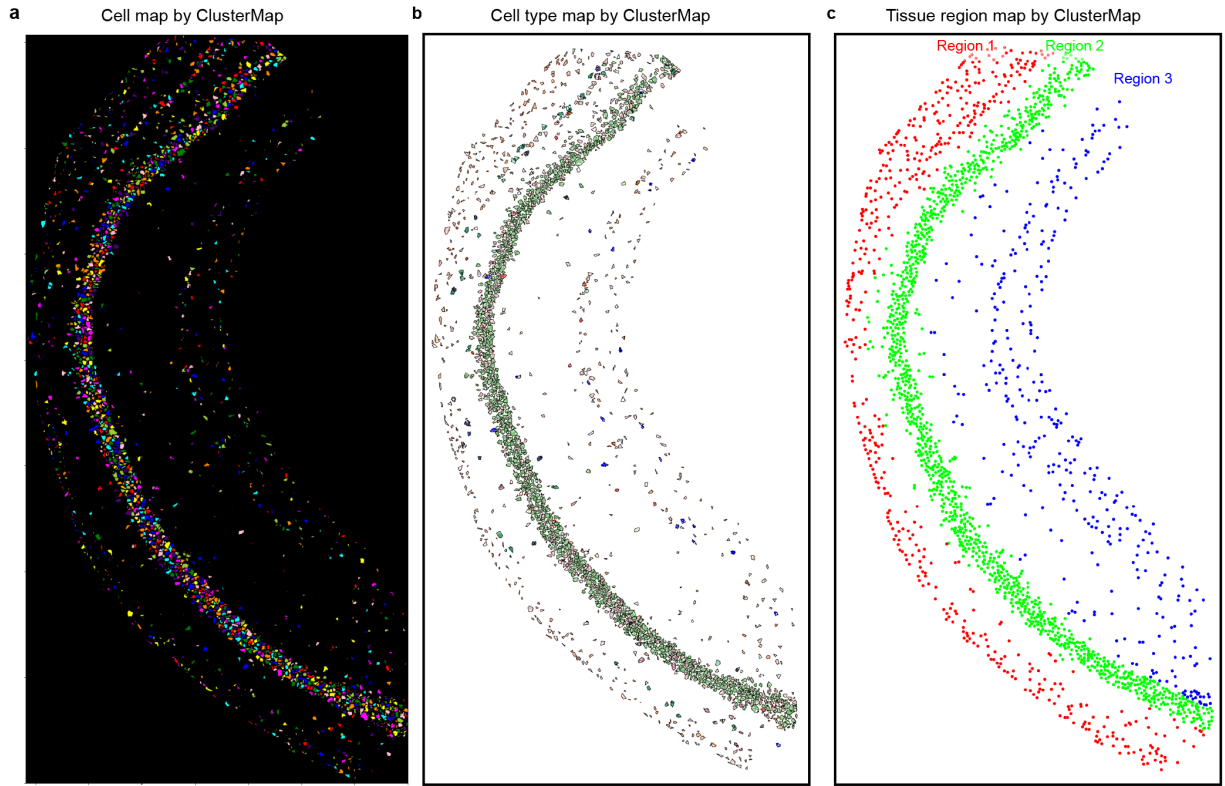
103 bottom heatmaps of cell niche composition sub-clustering are cell types in numbers annotated in

104 Figure 3.

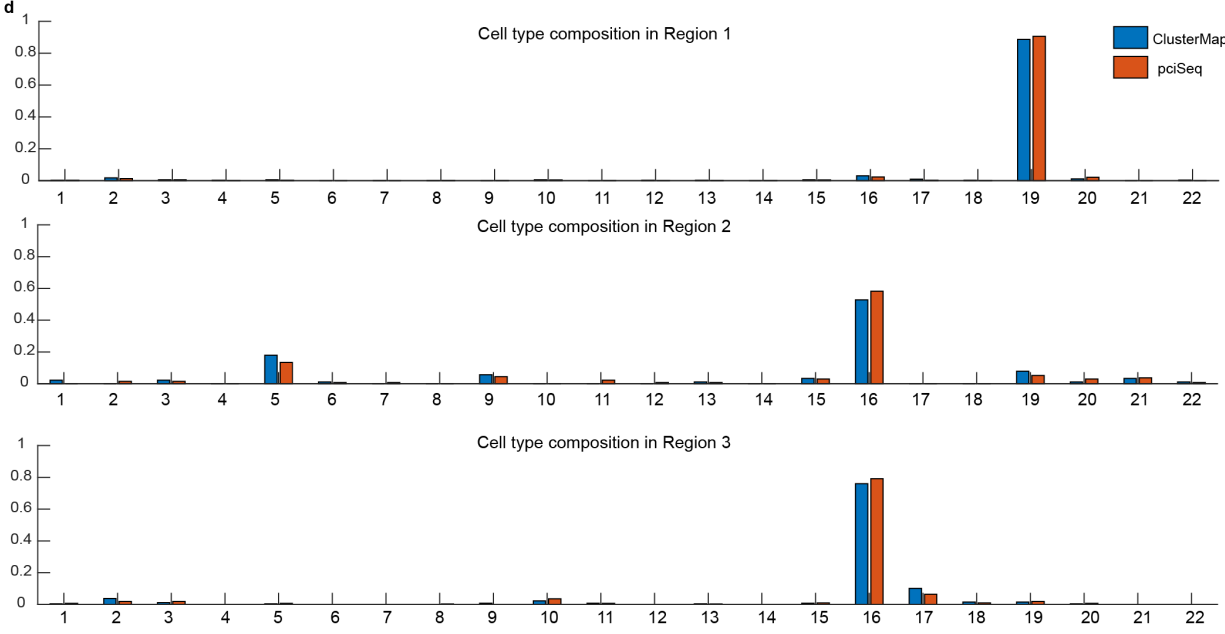
105

107 **Supplementary Figure 8**

108 **ClusterMap analyses across different experimental methods.** **a**, The cell segmentation map of
109 whole osmFISH mouse somatosensory cortex (SSp) datasets. Scale bar: 100 μm . **b,c**, UMAP and
110 heatmap visualization of 31 cell types in osmFISH datasets. **d**, The 2D cell segmentation map of
111 whole MERFISH mouse preoptic area (POA) datasets. Scale bar: 200 μm . **e,f**, UMAP and heatmap
112 visualization of 9 cell types in MERFISH datasets. The number of cells increased from 6,471 to
113 8,538 for osmFISH, from 2,620 to 2,924 for pciSeq, from 6,977 to 10,320 for MERFISH. The
114 number of reads increased from 1,248,106 to 1,690,328 for osmFISH, from 31,246 to 31,750 for
115 pciSeq, from 1,927,913 to 3,065,171 for MERFISH.

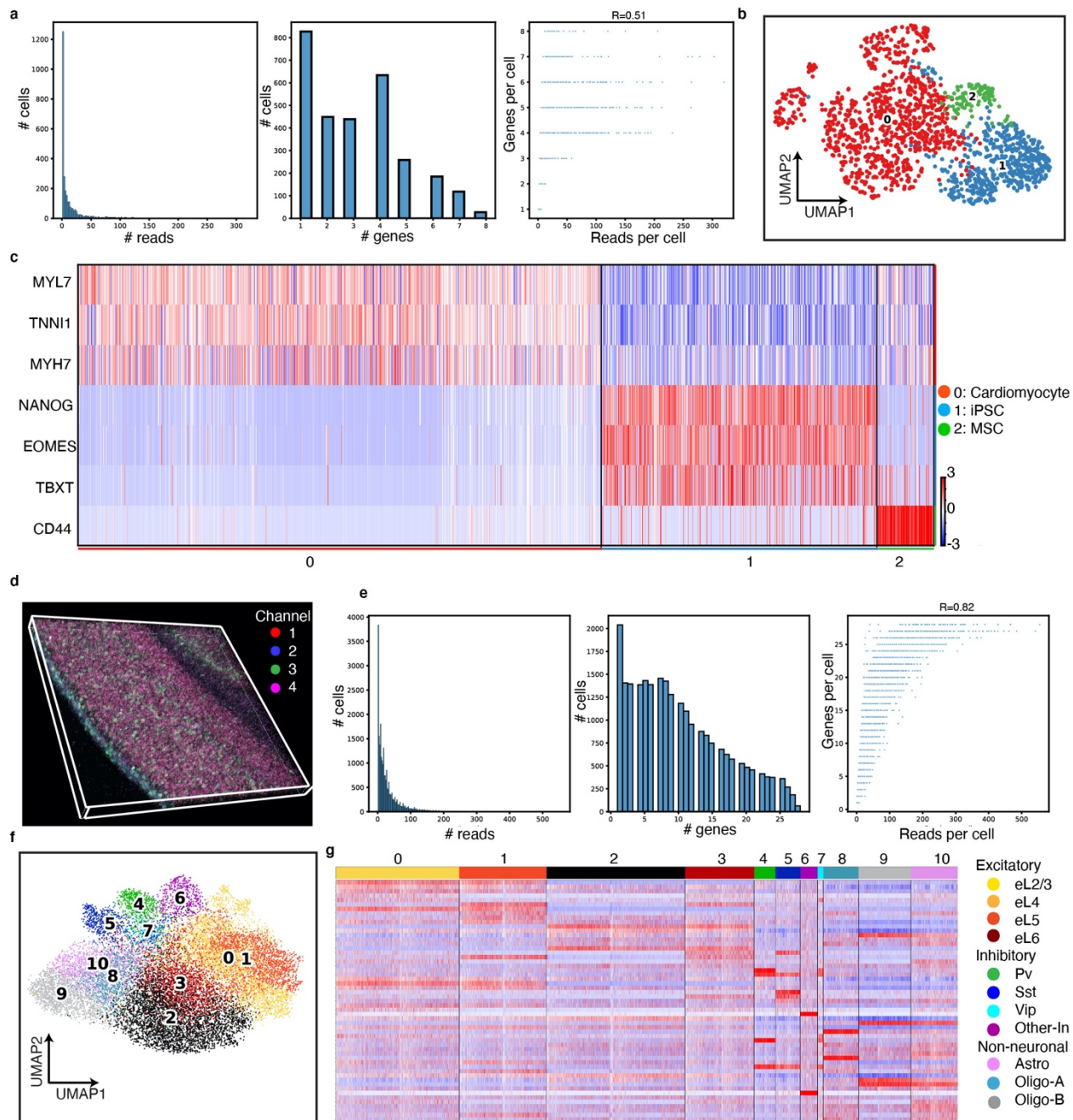


- 1: Axo-axonic
- 2: Basket
- 3: Bistratified
- 4: CGE IVY
- 5: CGE NGF
- 6: Cck Calb1/Slc17a8
- 7: Cck Cxcl 14+
- 8: Cck Vip Cxcl 14-
- 9: Cxcl14 NGC
- 10: Hippo
- 11: IS1
- 12: IS2
- 13: IS3
- 14: Ivy
- 15: MGE
- 16: Nonneuron
- 17: O-Bi
- 18: O/LM
- 19: PC CA1
- 20: PC other
- 21: Radiatum retrohip
- 22: Trilaminar
- Uncalled



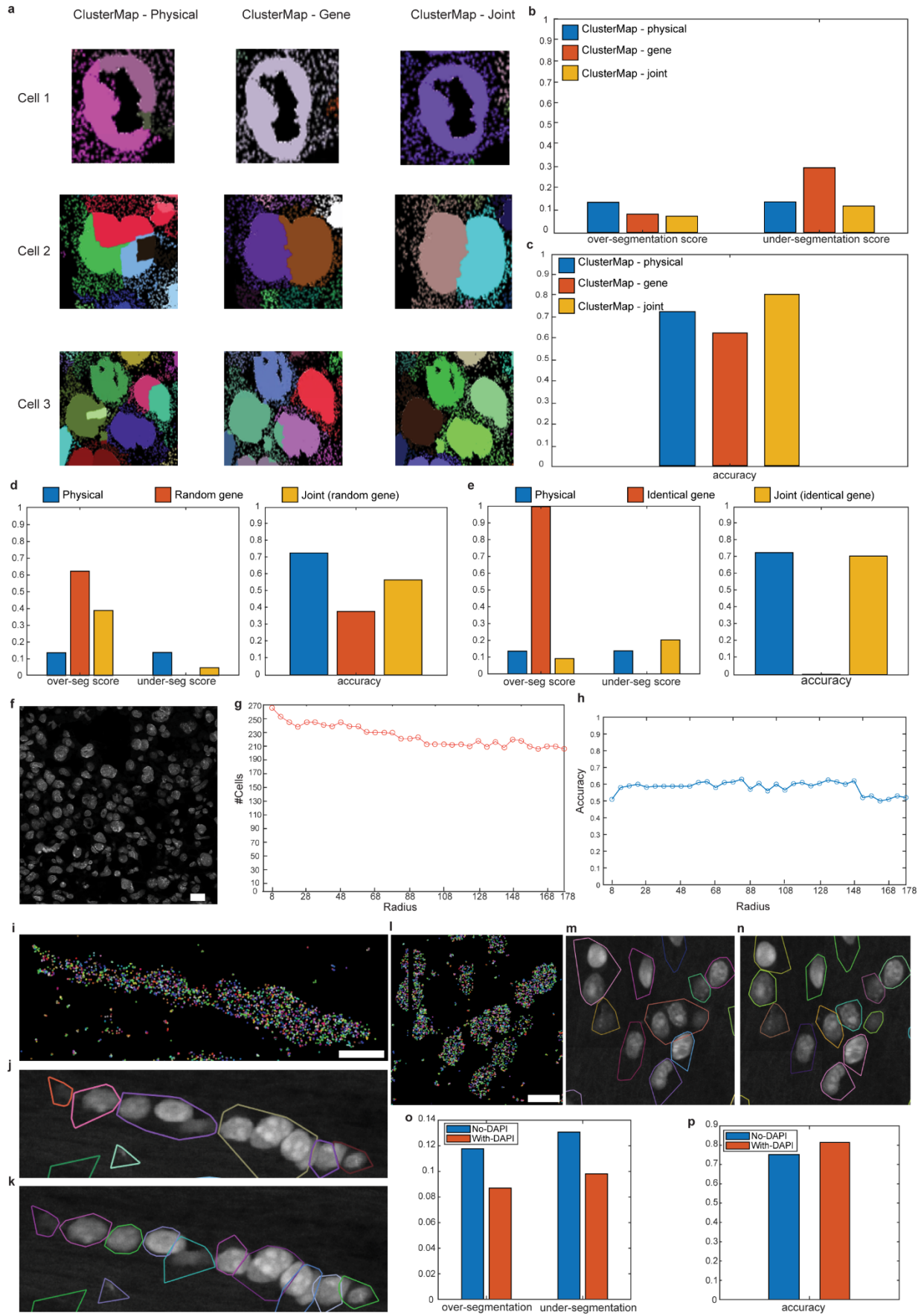
117 **Supplementary Figure 9**

118 **ClusterMap analyses of ISS data. a**, Cell segmentation map shows the cell segmentation results
119 by ClusterMap. Colors are randomly assigned to each cell mask. **b**, Cell type map shows the cell
120 type calling results. Colors are assigned according to their corresponding cell type categories. **c**,
121 Tissue region map shows laminar structure of hippocampus. Scale bar: 200 μm . **d**, Side-by-side
122 comparison of cell type compositions in each tissue region from ClusterMap and pciSeq of the ISS
123 data.



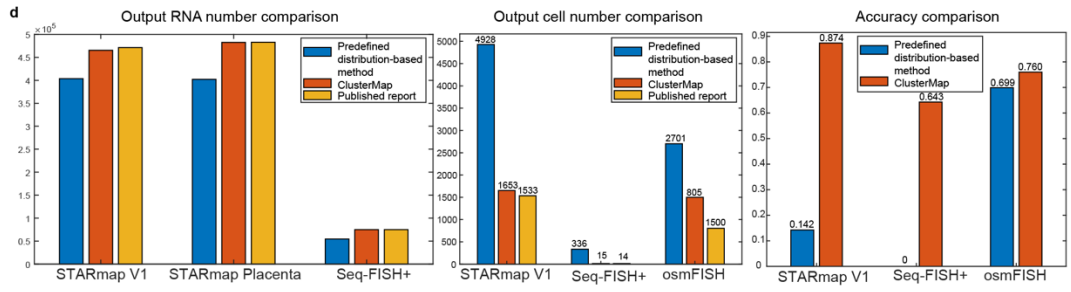
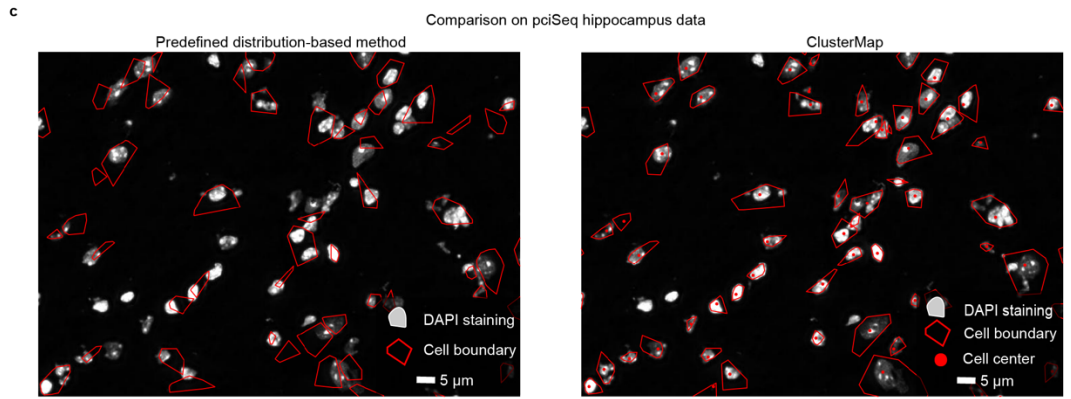
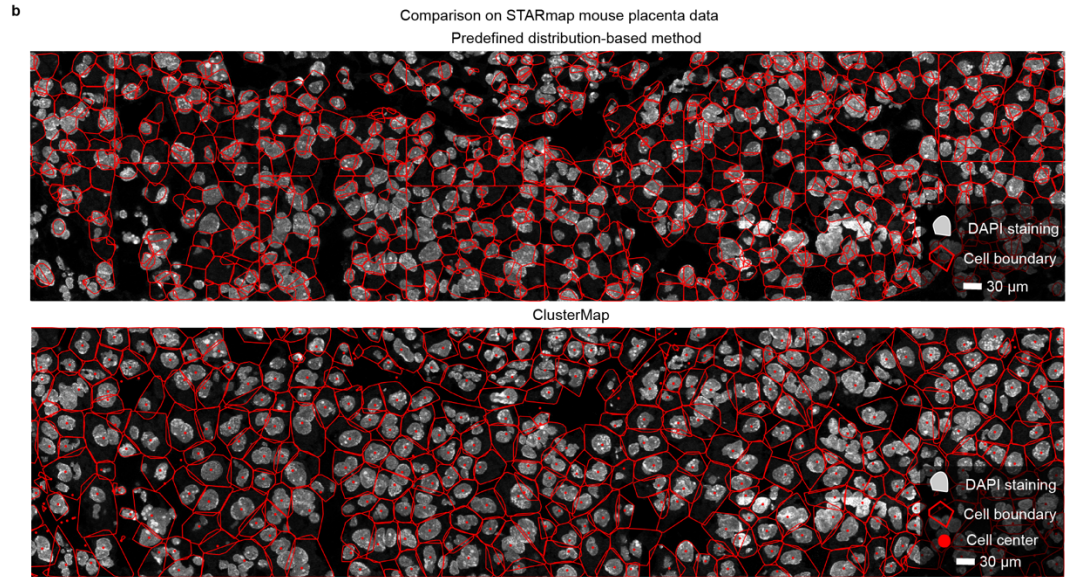
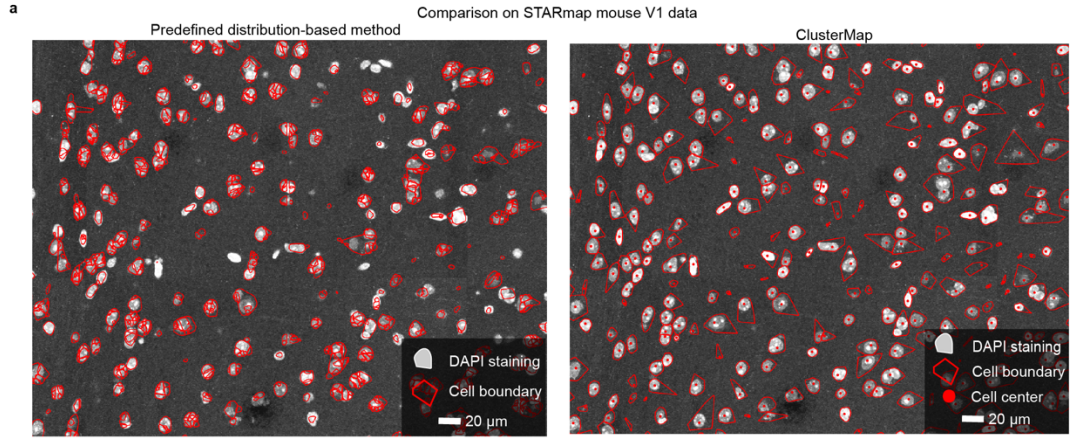
125 **Supplementary Figure 10**

126 **ClusterMap analyses in the 3D datasets. a**, Statistics of ClusterMap identified cells in the 3D
127 STARmap⁶ cardiac organoid²⁷ 8-gene dataset. Left: Histogram of detected reads (DNA amplicons)
128 per cell. Middle: Histogram of genes per cell. Right: Correlation plot between genes per cell and
129 reads per cell. **b, c**, UMAP and heatmap visualization of three cell types in the STARmap⁶ cardiac
130 organoid 8-gene dataset. The number of cells in each cell type is as follows: cardiomyocytes, 929;
131 induced pluripotent stem cells (iPSCs), 489; mesenchymal stem cells (MSCs), 101. **d**, 3D four-
132 channel composite raw fluorescent image of the first sequencing round shows spatial arrangement
133 of mRNA molecules in the STARmap⁶ mouse V1 28-gene dataset. Width 184 μm , height 194 μm ,
134 depth 100 μm . **e**, Statistics of ClusterMap identified cells in (**d**). Left: Histogram of detected reads
135 (DNA amplicons) per cell. Middle: Histogram of genes per cell. Right: Correlation plot between
136 genes per cell and reads per cell. **f, g**, UMAP and heatmap visualization of three cell types of (**d**).



138 **Supplementary Figure 11**

139 **Performance comparison of ClusterMap using physical density, gene distance, and joint**
140 **information. a**, Examples of cell segmentation using only physical density information (left), gene
141 (NGC) distance information (middle), and joint information (right). **b,c**, Bar plots demonstrating
142 the percentage of over-/under- segmented cells in ground truth cells (**b**) and overall accuracy (**c**)
143 in using physical distances information, gene (NGC) distance information, and joint information.
144 **d,e**, Bar plots demonstrating the percentage of over-/under- segmented cells in ground truth cells
145 (left) and overall accuracy (right) in using physical distances information, random (**d**) or identical
146 (**e**) gene (NGC) distance information, and joint information. **f**, Raw DAPI image of the targeted
147 mouse placenta tissue. Scale bar: 20 μ m. **g,h**, Line plots showing the number of cells and overall
148 accuracy to the radius. **i-m**, Two examples of the hippocampus regions in STARmap mouse V1
149 1020-gene datasets showing raw spatial transcriptomics data (**i,l**), ClusterMap results without
150 DAPI (**j,m**), and ClusterMap results with DAPI (**k,n**). Scale bar: 20 μ m. **o,p**, Bar plots showing
151 the percentage of over-/under- segmented cells (**o**) and overall accuracy (**p**) from ClusterMap
152 without and with DAPI.



154 **Supplementary Figure 12**

155 **Performance comparison of ClusterMap and other method across different types of *in situ***

156 **transcriptomic data. a,** Example of a region in the STARmap⁶ mouse V1 1020-gene dataset with

157 DAPI signals (gray) showing ground truth cell nuclei. Red contours show cell boundaries

158 identified by predefined distribution-based method²⁰ (left) and ClusterMap (right), respectively.

159 **b,c,** As in (a) but using the STARmap⁶ mouse placenta 903-gene dataset and published pciSeq⁴

160 dataset. **d,** Bar plots demonstrating the remaining RNA numbers, cell numbers and segmentation

161 accuracy for each dataset. In each bar plot, results from predefined distribution-based method²⁰,

162 ClusterMap, and published reports were shown in blue, red, and yellow, respectively.

163

164 **Supplementary Table**

165 **Supplementary Table 1.** Summary of the name, *in situ* sequencing protocol, number of genes,
 166 number of cells, number of reads, number of cell types, corresponding figures and note of 7
 167 datasets.

Dataset	Experimental Method	# Genes	# Cells	# Reads	# Cell types	Figures	Note
STARmap mouse V1 1020-gene	STARmap	1,020	1,599	863,426	16	Fig. 1c, Fig. 2, Supplementary Figs. 3,4,5	Source: Ref. 6. 2D analysis
STARmap mouse placenta 903-gene	STARmap	903	7,224	5,090,930	12	Fig. 3, Fig. 4, Supplementary Figs. 6,7	New data. 2D analysis
MERFISH mouse POA	MERFISH	140	10,320	3,065,171	9	Fig. 5, Supplementary Fig. 8	Source: Ref. 3. 3D analysis
pciSeq mouse hippocampus	ISS	98	2,924	31,750	23	Fig. 5, Supplementary Fig. 9	Source: Ref. 4. 2D analysis
osmFISH mouse SSp	osmFISH	33	8,538	1,690,328	31	Fig. 5, Supplementary Fig. 8	Source: Ref. 5. 2D analysis
STARmap cardiac organoid 8-gene	STARmap	8	1,519	47,594	3	Fig. 6, Supplementary Fig. 10	New data, 3D analysis
STARmap mouse V1 28-gene	STARmap	28	24,590	753,396	11	Fig. 6, Supplementary Fig. 10	Source: Ref. 6. 3D analysis

168